Proceedings World Geothermal Congress 2020+1
Reykjavik, Iceland, April - October 2021

Integrated Remote Sensing as a Tool in Determining Areas with High Geothermal Potential in the Amacan Geothermal Prospect, Philippines

Jeffrey T. Bermido, Kevin G. Guillermo, Oliver A. Briola, and Leonardo L. Morales

Energy Development Corporation, One Corporate Centre, Julia Vargas cor. Meralco Ave, Ortigas, Pasig City, Philippines

bermido.jt@energy.com.ph, guillermo.kg@energy.com.ph, briola.oa@energy.com.ph, and morales.ll@energy.com.ph

Keywords: remote sensing, geothermal exploration, lineament analysis, hydrothermal alteration, thermal mapping

ABSTRACT

Leonard is one of the active volcanoes in the Philippines, located in eastern Mindanao Island. It is interpreted to host the Amacan geothermal system characterized by Quaternary volcanism and favorable structural setting. In order to gain preliminary information on the prospect, remote sensing on the morphology, thermal anomalies, and zones of hydrothermal alteration were performed. Digital elevation models were processed to produce slope rasters which highlighted the geological features and topography. Major segments of the Philippine Fault and secondary structures were delineated, as well as caldera and domal features representing the potential heat sources. The Thermal Infrared Sensor (TIRS) Band 10 of Landsat 8 was also processed to generate the land surface temperatures. Thermal high anomalies were found to correlate with the distribution of the known thermal manifestations. The Operational Land Imager (OLI) bands of Landsat 8 were also processed using composite and band ratio operations to display the alteration zones and determine the alteration type. Using the Analytical Hierarchy Process (AHP) and Weighted Overlay Analysis in GIS, the remote sensing results were integrated to produce a geothermal potential map. Four areas were identified to have high geothermal potential and are recommended for more detailed assessments.

1. INTRODUCTION

The Leonard Volcano is classified by the Philippine Institute of Volcanology and Seismology (PHIVOLCS) as an active volcano, with its youngest tephra deposits dated 1,800 ka based on ^{14}C dating (Wood, 1980). Geothermal manifestations such as numerous hot and warm springs are distributed around the volcano, indicating the presence of a geothermal resource referred to as the Amacan system (Philippine Department of Energy, n.d.). Permeability in Amacan is facilitated by the active Philippine Fault which bifurcates into two in the area namely the Eastern Mindanao Fault in the west and the Mati Fault in the east (PHIVOLCS, 2015). Aside from its structural complexity, the Philippine Fault in Eastern Mindanao also forms a couple with the younging southward Philippine Trench (Quebral et al., 1996, Lallemand et al., 1998). The active status of this tectonic couple makes the area seismically active relative to the rest of the Philippine archipelago. Given this impressive geological framework, this study maximized the use of remote sensing and statistical tools in GIS to further understand the prospect and identify the areas of interest.

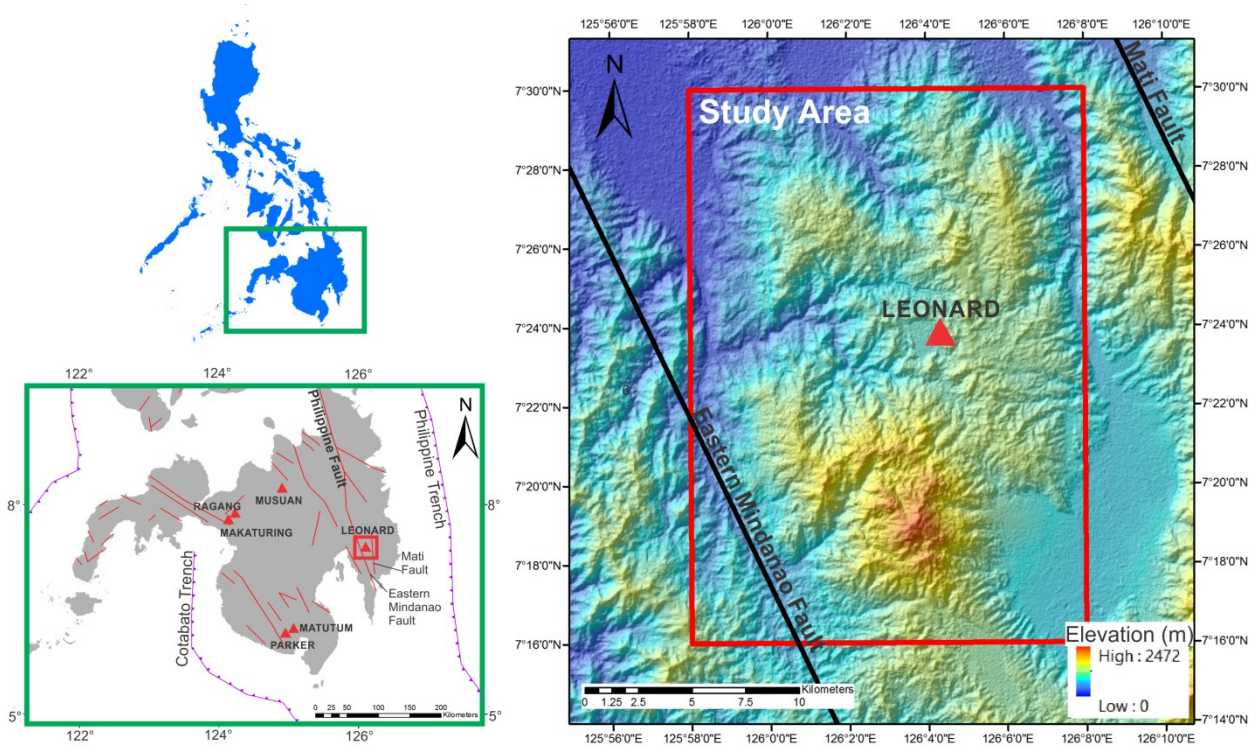

Figure 1: Location map and regional tectonic setting of the Amacan Geothermal Prospect (red box) in eastern Mindanao Island (green box), Philippines. Red triangles indicate active volcano locations. The prospect is bounded by the splays of the active Philippine Fault (Modified from PHIVOLCS, 2015).

2. MATERIALS AND METHODS

There are two materials used in this remote sensing study. The first dataset is the Digital Elevation Model (DEM) which was used in the morphological and lineament analysis. The DEMs were processed to produce hillshade, slope aspect, and slope gradient maps. Hillshade processing calculated the illumination value of a cell given a particular azimuth and altitude of a hypothetical light source. Slope aspect reflected the direction into where the slopes are facing. Lastly, slope gradient calculated the slope inclination or steepness of a surface in either degree or percentage values.

The second dataset is the Landsat 8 package of Eastern Mindanao with acquisition dated August 2015. This is comprised of Operational Land Imager (OLI) bands covering Bands 1-7 and Thermal Infrared Sensor (TIRS) bands covering Bands 10-11. As recommended by the US Geological Survey (2016), Band 11 was not used due to its large uncertainty factor. A series of steps based on Avdan and Javanovksa (2016) were applied to convert the OLI Band 10 using raster calculations in ArcGIS. This includes calculating the Top of Atmosphere Radiance, Brightness Temperature, Proportion of Vegetation, and the Normalized Difference Vegetation Index. The final Land Surface Temperature (LST) raster displayed areas with relatively higher temperatures relative to the background. The raster equation for the LST is as follows:

$$LST = \frac{BT}{1+w\left[\left(\frac{BT}{p}\right)(LSE)\right]} \quad (1)$$

where LST is the Land Surface Temperature, BT is the brightness temperature, and LSE is the land surface emissivity. W is the wavelength of emitted radiance at 11.5µm in the TIRS bands. The value of p to equal to 1.438 x 10-2 mK which was calculated using scientific constants - Planck's constant, Boltzmann constant, and the speed of light in vacuum. The process of generating LST maps was simplified by Buhari (2015).

The OLI bands were processed using ArcGIS Model Builder for the hydrothermal alteration mapping. Color composite processing was performed using ratio 5:7:6 to show the spatial distribution of hydrothermal alteration, following the method in Mia (2012). Band ratio operation, on the other hand, was carried out using Abrams ratio (6/7:4/3:5/6) to identify the type of alteration present.

To integrate the results, the Weighted Overlay Analysis in ArcGIS was used to identify zones with high geothermal potential. Four technical criteria were selected for the analysis namely: heat source, temperature, thermal manifestations, and structures. The weights of the criteria were determined from the Analytical Hierarchy Process (AHP), which considered the inputs of geothermal experts.

3. RESULTS AND DISCUSSIONS

3.1 Geomorphology and Potential Heat Sources

The digital elevation model in Figure 2.A was analyzed using several raster conversions in ArcGIS. Hillshade processing (Figure 2.B) was able to display the terrain variations in the area. The slope gradient map (Figure 2.C) showed the gradation of surface inclinations while slope aspect (Figure 2.D) showed the azimuth directions into where the slopes are facing.

The prospect encapsulates an oblong shaped terrane centered on Leonard Volcano (Figures 3). Previous geomorphologic interpretations by Paguican (2012) classified that this terrane is a volcanic massif given its low height/basal width ratio of 0.05, irregular plan shape, with intermediate to high ellipticity. The volcanic massif is characterized by moderately steep slopes with around 60% in the 18°-35° interval. An exception of this is the wide area east of Leonard which is differentiated by a smoother surface of slopes at 11°-18°. The more rugged terrain possibly reflects the extent of older volcanic deposits or the flank of older edifices. This is also supported by the radial drainage pattern surrounding the center, which is typical in volcanic systems. Contrarily, the smoother terrain east of Leonard represents the possibly younger volcanic deposits. These deposits have relatively less fault incisions and not as deep as the older deposits.

The slope aspect map also shows the differences between the old and young deposits within the massif. The older deposits are characterized by slopes facing the northeast. The younger deposits on the other hand have no dominant slope directions. Paguican and Bursik (2016) explained that areas having slopes facing in many directions may indicate rough material deposits, such as emplaced lava flows or avalanche and slide toes.

The raster images were also able to highlight the surface expressions of potential heat sources in the area (Figure 3). The most prominent of which is the Leonard Caldera which forms a conspicuous circular feature at the center of the prospect. The magma chamber responsible for the caldera-forming eruption may serve as the main heat source that drives the Amacan geothermal system. This heat source is also possibly expressed at the surface by a dome located at the southeastern rim of the Leonard Caldera named in this study as the Leonard South Dome. Other dome features in the prospect are Manat Dome located north of the Leonard Caldera, Masara Dome located west, Ugos Dome located south, and Maraut Dome located further southwest.

All these potential heat sources show young morphological characteristics that may indicate concurrence with the development of the geothermal system in Amacan. These caldera and domes show minimal dissection of structures and relatively lower degree of erosion. A larger caldera named as the Masara Caldera (Figure 4) was also delineated but it showed relatively more eroded morphology and may not be related to the current geothermal system. The Masara Caldera represents an ancient locus of volcanism and magmatism which is presently being mined and explored for mineral deposits. This old caldera structure may be irrelevant to the heat source of the geothermal system in Amacan.

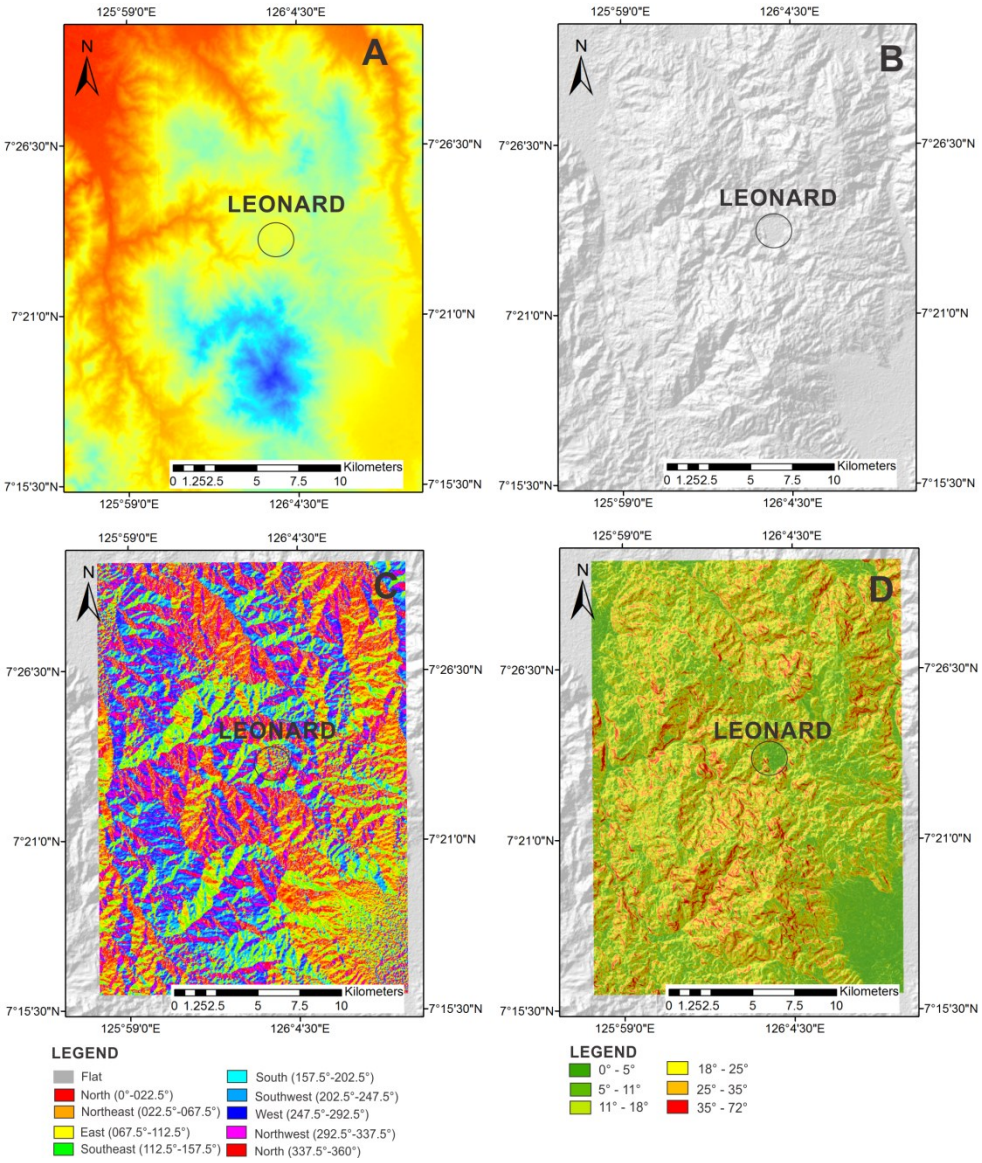

Figure 2: A) Unprocessed DEM B) Hillshade C) Slope Aspect D) Slope Gradient

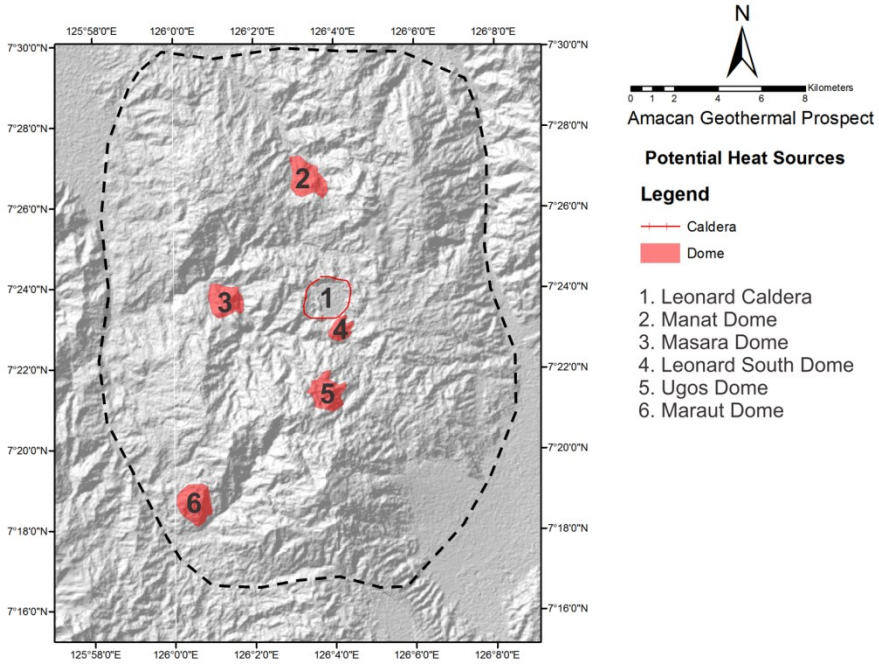

Figure 3: Potential Heat Sources in the Amacan prospect. Dashed line refers to the trace of the massif by Paguican (2012).

3.2 Lineament Analysis

In geothermal areas situated in tectonically active regions such as the Philippines, secondary permeability from faults and fractures is recognized as the main control for fluid flow, compared with the primary permeability of the formation. It is crucial then to map the structures and characterize its permeability as these serve as the main targets for geothermal drilling. The first step in the structural characterization process is to delineate the structures from processed digital elevation models. Figure 4 shows the hillshade image with the drawn lineaments and arcuate features. Combined hillshade, slope aspect, and slope gradient was used to determine the trace of the structures.

The major structures in the Amacan Geothermal Prospect commonly form kilometers of valleys and topographic breaks. These geomorphologic expressions of structures also influence the drainage pattern in the area. The largest structures are the segments of the Philippine Fault such as the Eastern Mindanao Fault. A sinistral sense is postulated for these structures being consistent with the general sinistral kinematics of the Philippine Fault. The next two most prominent structures are Manat Fault and Amacan Fault which strike at about 315° azimuth. Manat Fault mainly controls Manat River while Amacan Fault has its best geomorphologic expression along Malumon River. Theoretical predictions from wrench tectonics of the main splays of the Philippine Fault indicate that these two major structures would have a similar sinistral sense as synthetic shears.

Another important structure is the E-W trending Masara Fault which almost crosses the entire latitude of the prospect. The structure is prominent from hillshade images and has a strike of 95° azimuth. Theoretical predictions show that structures of this orientation would have a tensional character being parallel to the maximum horizontal stress in Mindanao. Two parallel NE-SW trending structures also cut the prospect namely the Lumanggang and Maraut Faults. Lumanggang Fault has its most obvious trace west of Leonard Caldera while Maraut Fault has its main trace along Maraut River. Antithetic sense is predicted for this structural orientation. Notable N-S trending structures are delineated near the western and eastern borders of the prospect, forming the largest river systems namely Hijo and Agusan Rivers. Both Hijo and Agusan River Faults juxtapose the volcanic massif with the terranes at the west and east. Theoretical prediction of these structures indicates compression being perpendicular to the maximum horizontal stress.

Aside from linear structures, there are also three arcuate features which may represent the distribution of old and young volcanic centers. The largest of which is Masara Caldera, which measures for about nine kilometers in diameter and has a north-south elongation. Within the Masara Caldera is the circular Leonard Caldera which primarily appears to host the heat source of the Amacan system. A collapse feature named as the Maraut Collapse is also observed on the southern rim of the Masara Caldera. The collapse feature has a NE-SW elongation following the configuration of the Maraut Fault.

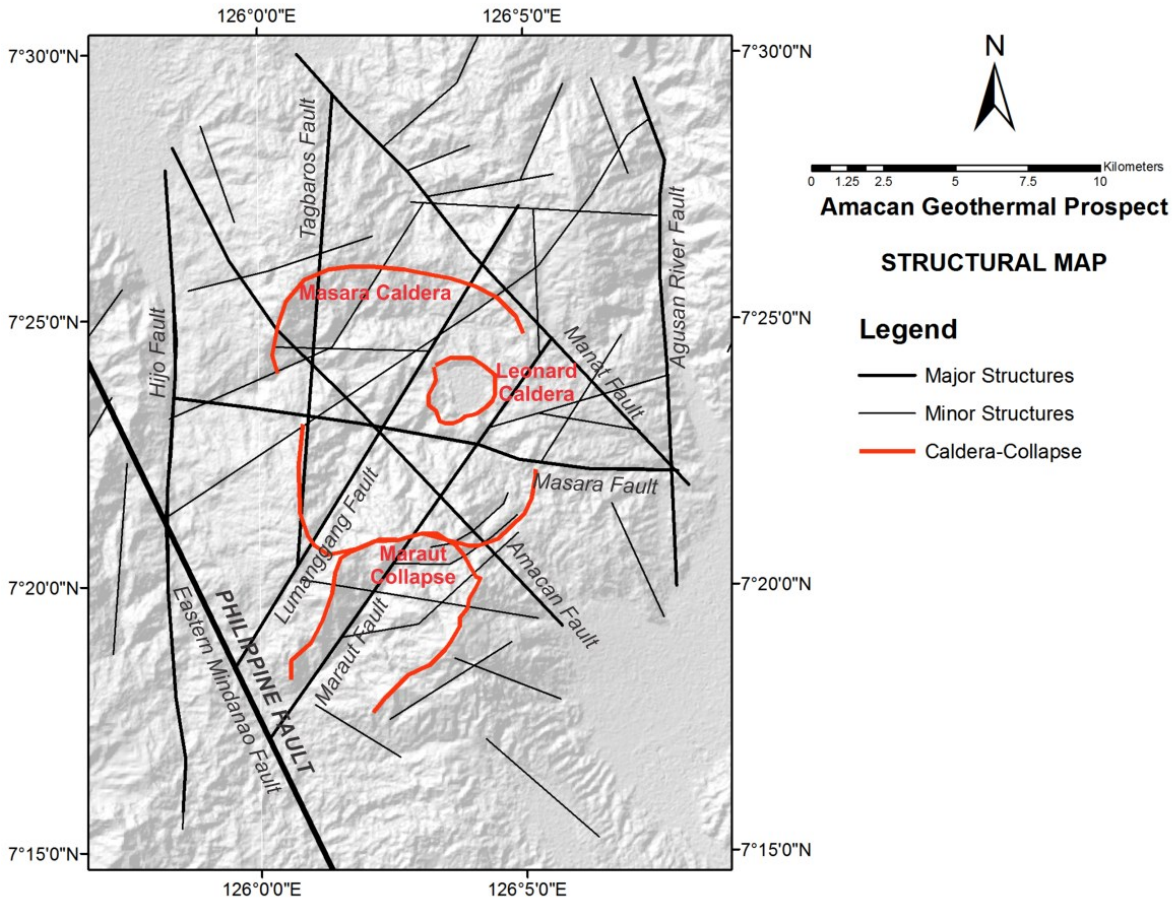

Figure 4: Remote sensing-based structural map of the Amacan Geothermal Prospect

3.3 Thermal Mapping

Land surface temperature (LST) is defined as the skin temperature of the land surface or the temperature felt when the ground is touched (Avdan and Jovanovska, 2016). The LST map (Figure 5.E) was generated using a series of raster calculations as presented by Figures 5.A to 5.D. As shown in the final map, thermal highs are displayed in warmer reddish coloration while relatively colder areas are in blue. The maximum temperature calculated is about 30°C, which is similar with other land surface temperature maps in other geothermal areas (Meneses, 2015).

Figure 5.E also shows the documented locations of thermal manifestations in the area such as hot and warm springs according to the Philippine Department of Energy. A linear high temperature anomaly is observed near the Manat-Bucal thermal springs. More widespread anomalies are found in the locations of the Leonard-Mainit-APEX, Maragusan, Maraut, and Amacan thermal areas. Contrarily, relatively colder areas are observed in the northwest, northeast, and central-south portion of the prospect. This may be due to thick vegetation or the lack of geothermal activity at the surface. For reference, the TIRS band was also captured in the morning given the sun elevation of 67°.

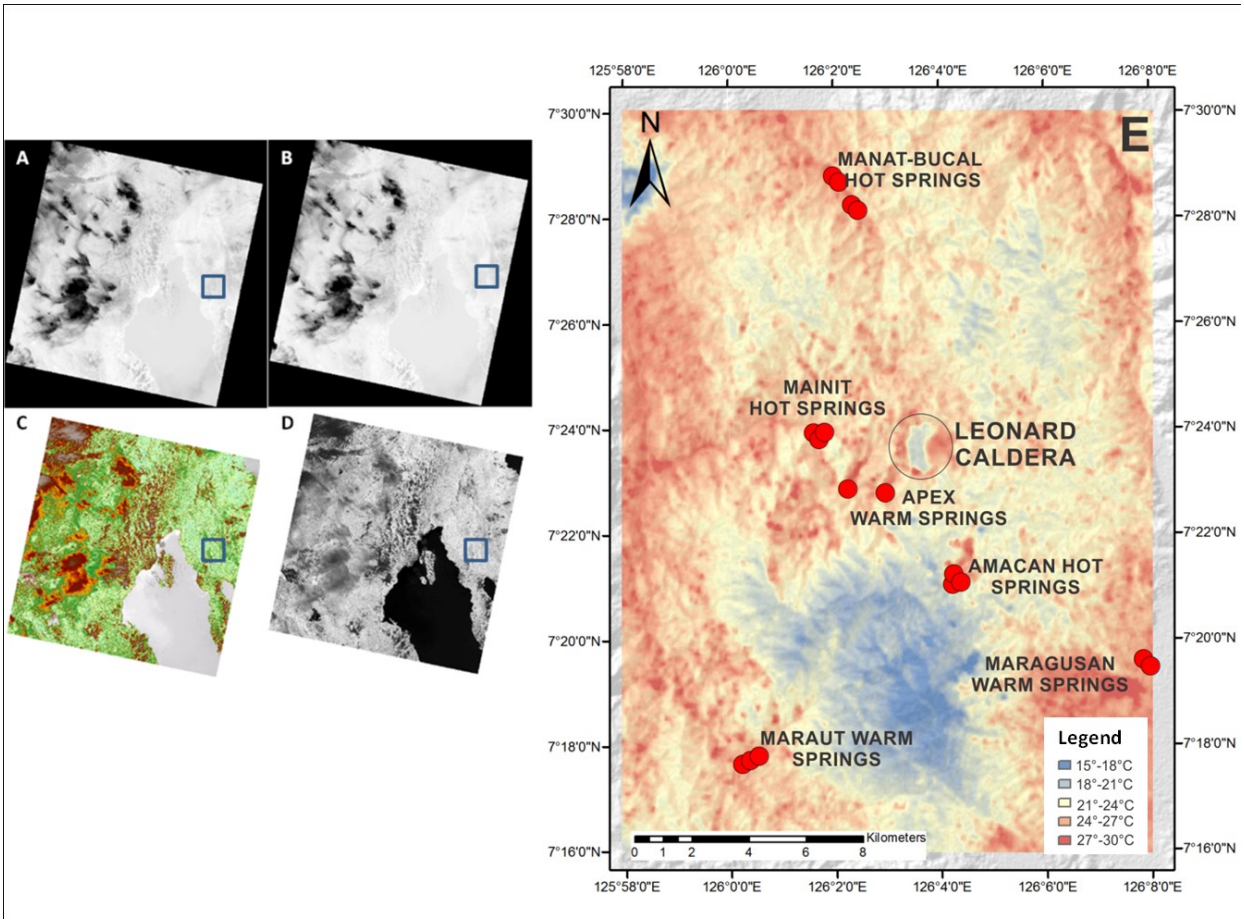

Figure 5: Raster calculations converting Band 10 to Land Surface Temperature. The prospect is highlighted by the blue boxes. (A) Top of Atmosphere Radiance (B) Brightness Temperature (C) Normalized Difference Vegetative Index (NDVI) (D) Land Surface Emissivity (E) Land Surface Temperature Map with documented thermal areas in red circles (DOE, n.d.).

3.4 Hydrothermal Alteration Mapping

Previous studies explained the fact that certain minerals associated with hydrothermal processes, such as iron-bearing minerals (e.g., goethite, hematite, jarosite, and limonite) and hydroxyl bearing minerals (e,g. kaolinite and K-micas) show diagnostic spectral features that allow their remote identification (Hunt, 1980; Mia, 2012). Iron oxide is said to be a common constituent of alteration zones associated with hydrothermal sulfide deposits (Poormirzaee and Oskouei, 2009). The major iron oxide species, formed from the weathering of sulfides, absorb energy at different frequencies providing a means of discrimination using hyperspectal scanners (Taranik et al., 1991). Hydroxyl bearing minerals on the other hand form the most widespread product of alteration.

Using OLI bands of Landsat 8, hydrothermal alteration maps were generated as shown by Figure 6. Composite ratio operation 5:7:6 remotely identified areas with hydrothermal alteration in the study area. The spatial distribution of altered grounds is observed along major drainages where the reflectance is coming from either the altered exposed bedrock or fluvial deposits with altered material. Hydrothermal alteration is also evident in mining areas south of the Leonard Caldera and near thermal areas. Specifically, wider distribution of hydrothermal alteration is observed along Manat-Bucal, Maraut, Mainit-APEX, Amacan, and around Leonard Caldera.

Abrams ratio (6/7:4/3:5/6) was able to differentiate the type of alteration minerals present (Figure 6). Iron-oxide minerals such as limonite, hematite, and jarosite were discriminated as yellow to yellow-green while hydroxyl bearing minerals such as clays appeared as red. As with band ratio operation, alteration zones are mapped along major drainages, known thermal areas, and altered outcrops.

The widest iron oxide altered area is in Mainit-APEX while the widest clay altered area is observed in Amacan. The purple coloration which dominates the resulting image corresponds to the background that is possibly unaltered or vegetated with no exposures.

Given the presence of mining areas across the prospect, there is high uncertainty as to whether these alteration zones are related to the active geothermal system or associated with the fossil hydrothermal systems in the area. The proximity of the Leonard Volcano with respect to the mining districts to the south would indicate that alteration overprinting is expected. Therefore, it is crucial to ground-verify these observations from remote sensing to ascertain that the hydrothermal alteration is geothermal-related.

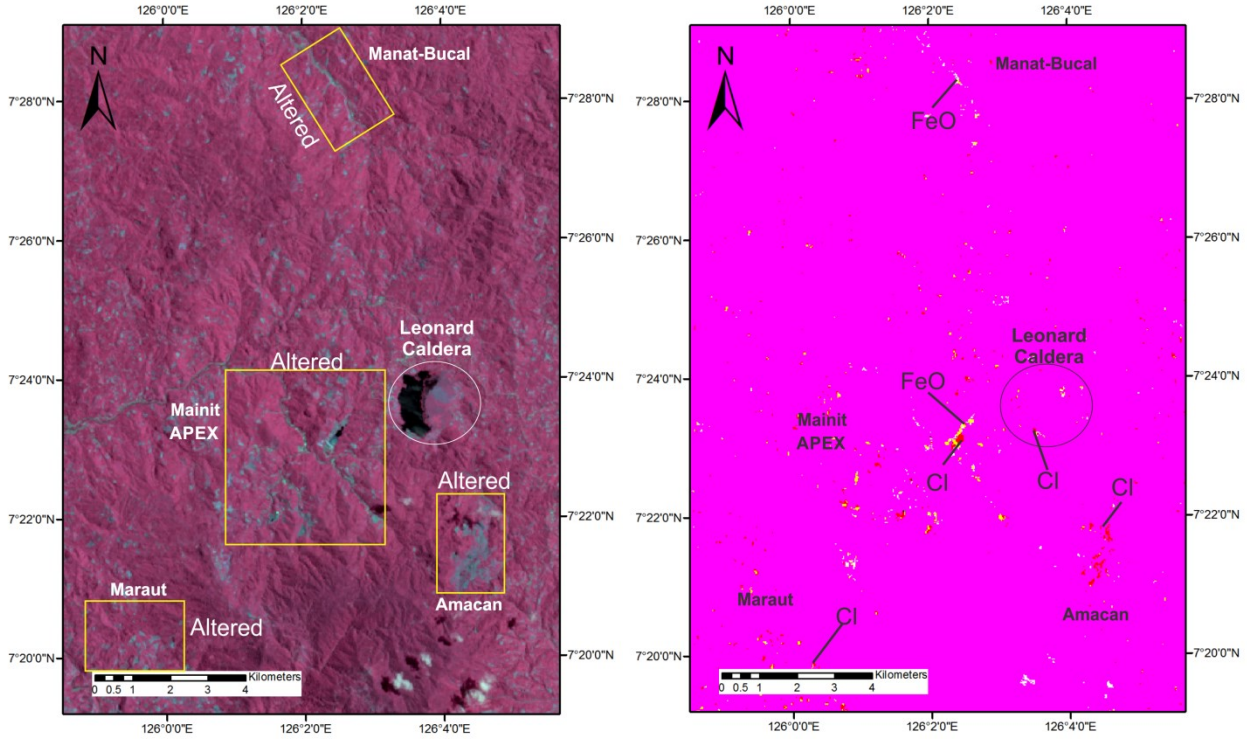

Figure 6: Left: Composite ratio operation 5:7:6 showing areas that are hydrothermally altered. Right: Abrams ratio operation (6/7:4/3:5/6) distinguishing iron oxide (FeO) and clay (Cl) minerals

4. INTEGRATED REMOTE SENSING AND RECOMMENDED PRIORITY AREAS FOR EXPLORATION

The weighed overlay analysis tool in ArcGIS was used to integrate the remote sensing results and identify zones of high geothermal potential, following the similar methods in Jander (2015) and Chaudhari et al. (2018). Four criteria indicating geothermal potential were selected for the analysis namely heat source, geological structure, temperature, and thermal manifestations, which represent the remote sensing data generated in this study. Hydrothermal alteration was not selected as a criterion given the high uncertainty on whether the displayed alteration is related to the current geothermal system or from the known fossil hydrothermal systems in the area. Given that the heat source, structure, and thermal manifestation data are single objects or features in the GIS environment, Euclidean distance tool was used to generate rasters that would show the measured distance from every cell to these objects as presented in Figure 7. This implies that an area of high geothermal potential has the least Euclidean distances with respect to a heat source, structure, and thermal manifestations. With regards to temperature, an area of high geothermal potential would also have the highest values with reference to the land surface temperatures generated.

Pairwise comparison using the Analytical Hierarchy Process (AHP) was used to derive the weights for the four criteria such as in Yalcin and Gul (2017). The AHP is a widely used tool by researchers and decision makers in which many criteria are considered in the prioritization of alternatives. The process has already been applied in geothermal context (Suryantini and Wibobo, 2010). Comparison of the four criteria by geothermal experts led to the consolidated results presented in Table 1. As Amacan is postulated to be a high temperature system, the weights given for heat source and temperature are at 30% signifying the equal importance of the two criteria. Lower weights of 20% were given to thermal manifestations and structures. The four weights generated were then used in the weighted overlay analysis in ArcGIS through its ModelBuilder.

Figure 8 shows the final geothermal potential map which highlights the high potential zones in red within the study area. These are Leonard-Mainit-APEX, Amacan, Manat-Bucal, and Maraut. Moderate potential in orange are mapped around these high potential zones. Low to no geothermal potential areas are displayed in green. Figure 9 focuses on the four areas and presents the overlaps of data on structure, heat source, temperature, thermal manifestations, and hydrothermal alteration.

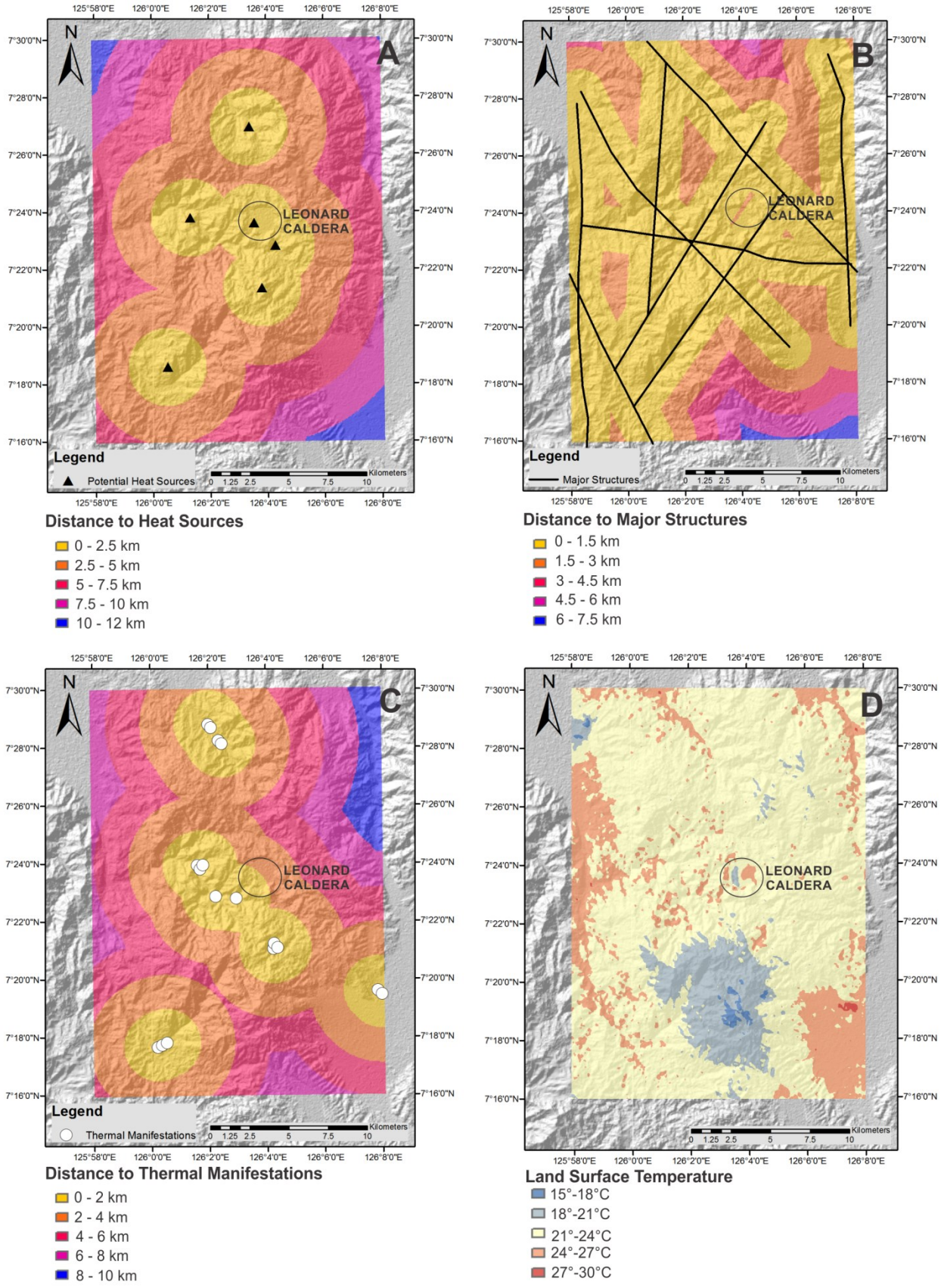

Figure 7: Thematic Layers for the Weighted Overlay Analysis. (A) Euclidean distance to heat sources (black triangles) (B) Euclidean distance to major structures (black lines) (C) Euclidean distance to thermal manifestations (white circles) (D) Land Surface Temperature Map.

Criteria	Classes	Ranks	Weights
Euclidean Distance to Heat Source	0-2.5 km	1	**30%**
	2.5-5 km	2	
	5-7.5 km	3	
	7.5-10 km	4	
	10-12 km	5	
Euclidean Distance to Major Structure	0-1.5 km	1	**20%**
	1.5-3 km	2	
	3-4.5 km	3	
	4.5-6 km	4	
	6-7.5 km	5	
Land Surface Temperature	15-18°C	5	**30%**
	18-21°C	4	
	21-24°C	3	
	24-27°C	2	
	27-30°C	1	
Euclidean Distance to Thermal Manifestation	0-2 km	1	**20%**
	2-4 km	2	
	4-6 km	3	
	6-8 km	4	
	8-10 km	5	

Table 1: Criteria Used in the Weighted Overlay Analysis and the Weights from the Analytical Hierarchy Process

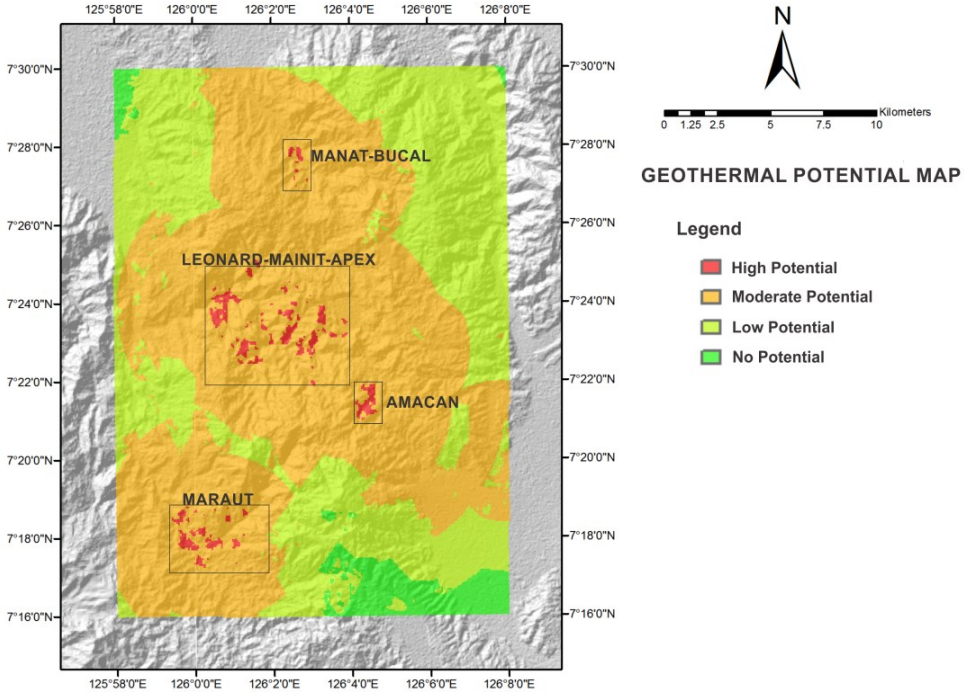

Figure 8: Final Geothermal Potential Map of the Amacan Geothermal Prospect from the Weighted Overlay Analysis

The largest area showing high geothermal potential is the Leonard-Mainit-APEX block (Figure 9.A) which measures for about 6 km x 7.5 km. The potential heat sources in this block are represented by the Leonard Caldera, Masara Dome, and Leonard South Dome. The block also shows the highest degree of fault confluence with Amacan Fault, Maraut Fault, Lumanggang Fault, and Masara Fault transecting the area. Thermal manifestations such as the Mainit hot springs and APEX warm springs are also enclosed by this block. High temperatures in discrete patches are also observed from the land surface temperature map. As this block is proximal to mining districts, certainty on geothermal-related alteration is only placed at the rims of the Leonard Caldera and near thermal manifestations.

About three kilometers south of Leonard Caldera is the Amacan block (Figure 9.B). The potential heat source of this block is the Ugos Dome which is reported to have an upflow (DOE, n.d.). East of the Ugos Dome is the coincidence of a large thermal anomaly body with extensive clay alteration and the occurrence of hot springs. Two major structures traverse the area namely the Amacan Fault and the Maraut Fault. The block is also located at the southeastern rim of the old Masara Caldera, with ring fractures also observed in the area.

The Manat block at the north (Figure 9.C) is characterized by the Manat Dome as a potential heat source. The main structure in this block is the Manat Fault, where thermal anomalies and alteration zones are similarly oriented. Several hot springs are also documented along this fault, signifying that the Manat block may be largely controlled by the Manat Fault. Lastly, the Maraut block at the southwest (Figure 9.D) has the Maraut Dome as the potential heat source. Several warm springs are documented south of the dome, which also follow the trend of the Maraut Fault. Permeability in this block may have offered by the Eastern Mindanao Fault, Lumanggang Fault, and the Maraut Collapse. Patches of thermal anomalies and hydrothermal alteration are also observed in the area.

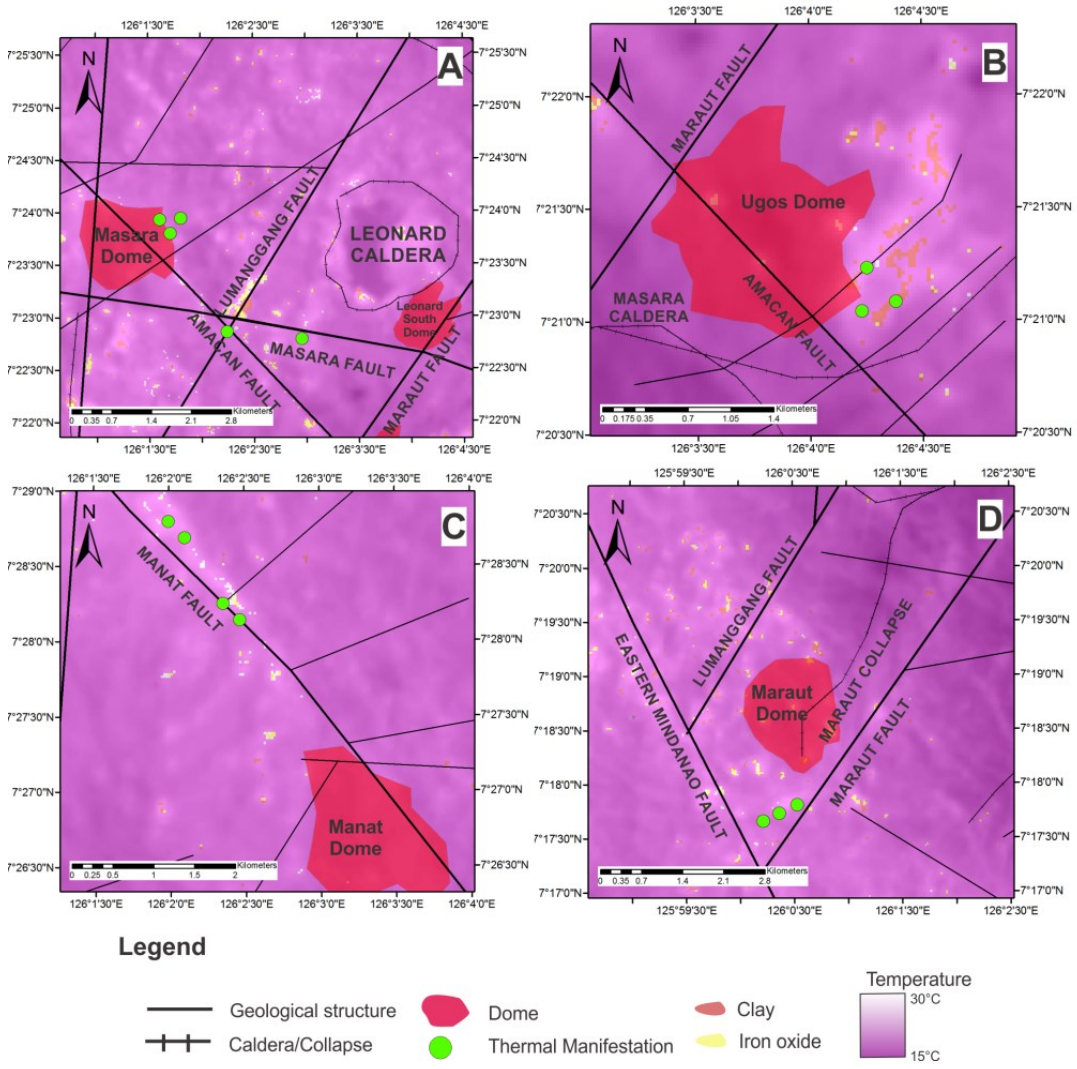

Figure 9: The four areas with high geothermal potential in the Amacan geothermal prospect. A) Leonard-Mainit-APEX B) Amacan C) Manat-Bucal D) Maraut

5. SUMMARY AND CONCLUSIONS

The study integrated known remote sensing methods to gain preliminary information on the Amacan Geothermal Prospect and identify areas of interest. Geomorphologic analysis from slope aspect, slope gradient, and hillshade identified two major terrains representing the variations in deposits within the massif. Heat sources such as young volcanic centers and domes were also identified from the geomorphologic analysis. The most prominent of which is the Leonard Caldera being the youngest eruptive center in the area. Lineament analysis revealed that the major structures are oriented NW-SE, NE-SW, N-S, and E-W. The major structures are

the segments of the Philippine Fault and its second order faults produced from postulated wrenching. Three arcuate features are also identified namely the old Masara Caldera, young Leonard Caldera, and the elongate Maraut Collapse.

Thermal mapping showed areas of high temperatures relative to the background, especially near thermal areas and open grounds with mining activity or lack of vegetation. The highest temperature measured is 30°, similar with other geothermal areas in the Philippines. Hydrothermal alteration mapping was also able to discriminate iron oxide and clay alteration. Notable hydrothermal alteration zones are mainly found at the center of the prospect. Using the weights derived from the Analytical Hierarchy Process for the four selected criteria in evaluating high temperature systems, the weighted overlay analysis in GIS narrowed down the large prospect into four priority areas namely: Leonard-Mainit-APEX, Amacan, Manat-Bucal and Maraut.

Overall, remote sensing was able to serve as a tool in determining areas with high geothermal potential and activity using freely available datasets. This study however stresses the importance of ground validation to calibrate the remote sensing process. Given that the area also hosts mining districts, the anomalies may not just reflect the current hydrothermal system but from the paleo-hydrothermal systems as well.

REFERENCES

Avdan U. and Jovanovska G. (2016) Algorithm for Automated Mapping of Land Surface Temperature Using LANDSAT 8 Satellite Data; *Journal of Sensors*, Volume 2016

Buhari, U. (2015). Landsat 8: Estimating Land Surface Temperature Using ArcGIS. Retrieved September 22, 2017, from https://www.youtube.com/watch?v=uDQo2a5e7dM

Chuadhari, R.V., Lal, D., Dutta, S., Umrikar, B., and Halder, S. (2018) Weighted Overlay Analysis for delineation of ground water potential zone: A Case Study by Pirangut River Basin. *International Journal of Remote Sensing & Geoscience*, Volume 7 Issue 1

Department of Energy. (n.d.). Amacan Geothermal Prospect. Retrieved July 1, 2019, from https://www.doe.gov.ph/amacan-geothermal-prospect

Hunt G. R. (1979) Near Infrared (1.3–2.4 μm) spectra of alteration minerals – potential for use in remote sensing; *Geophysics* 44 1974–1986.

Jander, N. (2015). ArcGIS Suitability Analysis: Forestry. Retrieved October 5, 2019, from https://www.youtube.com/watch?v=uDQo2a5e7dM

Jensen J. R. (1996) Introductory digital image processing: A remote sensing perspective; 2nd edition, Prentice Hall Series in Geographic Information Science; 318p.

Lallemand, S., Popoff, M., Cadet, J.-P., Deffontaines, B., Bader, A.G., Pubellier, M. and Rangin, C., (1998) The junction between the central and southern Philippine Trench. *Journal of Geophysical Research*, 103, 933−950.

Meneses, S.M., (2015). Thermal Remote Sensing at Leyte Geothermal Production Field using Mono-window Algoriths. *Proceedings* World Geothermal Congress. Melbourne, Asutralia.

Mia, B., & Fujimitsu, Y. (2012). Mapping hydrothermal altered mineral deposits using Landsat 7 ETM+ image in and around Kuju volcano, Kyushu, Japan. *Journal Earth System Science* , 1049-1057.

Paguican E.M.R. (2012). The structure, morphology, and surface texture of debris avalanche deposits: field and remote sensing mapping and analogue modelling. *Earth Sciences*. Université Blaise Pascal - Clermont-Ferrand II.

Paguican E.M.R and Bursik M.I. (2016) Tectonic Geomorphology and Volcano-Tectonic Interaction in the Eastern Boundary of the Southern Cascades (Hat Creek Graben Region), California, USA. Front .EarthSci.4:76.

PHIVOLCS (2015). Distribution of active faults and trenches in the Philippines

Suryantinti and Wibobo H.. (2010) Geothermal Prospect Selection Using Analytical Hierarchy Process (AHP): A Case Study in Sulawesi Island, Indonesia; *Jurnal Geologi Indonesia*, Volume 5 No. 4

Quebral, R., Pubellier, M. and Rangin, C., (1996). The onset of movement on the Philippine fault in eastern Mindanao: A transition from a collision to strike slip environment. Tectonics, 15, 713−726.

Taranik D. L., Kruse F. A., Goetz A. F. H. and Atkinson W.W. (1991) Remote sensing of ferric iron minerals as guides for gold exploration; *Proceedings* Eighth Thematic Conference on Geologic Remote Sensing, Denver, Colorado, pp. 197–228.

US Geological Survey (2016). Landsat 8 Data Users Handbook

Wood, P. (1980). A Report on a visit to the Philippines, February 1980. Unpublished report. NZ DSIR, 1980.

Yalcina M. and Gul, F.K (2017) A GIS-based multi criteria decision analysis approach for exploring geothermal resources: Akarcay basin (Afyonkarahisar). *Geothermics*, Volume 67, Pages 18-28